arXiv:1610.00252v1 [cond-mat.dis-nn] 2 Oct 2016

Chaos and correlated avalanches in excitatory neural networks with synaptic plasticity

Fabrizio Pittorino,[1,2] Miguel Ibáñez-Berganza,[2] Matteo di Volo,[3] Alessandro Vezzani,[4,1] and Raffaella Burioni[1,2,*]

[1] *Dipartimento di Fisica e Scienza della Terra, Università di Parma, via G.P. Usberti, 7/A - 43124, Parma, Italy*
[2] *INFN, Gruppo Collegato di Parma, via G.P. Usberti, 7/A - 43124, Parma, Italy*
[3] *Group for Neural Theory, Laboratoire de Neurosciences Cognitives, INSERM U960, École Normale Supérieure, Paris, France*
[4] *IMEM-CNR, Parco Area delle Scienze, 37/A-43124 Parma, Italy*

A collective chaotic phase with power law scaling of activity events is observed in a disordered mean field network of purely excitatory leaky integrate-and-fire neurons with short-term synaptic plasticity. The dynamical phase diagram exhibits two transitions from quasi-synchronous and asynchronous regimes to the nontrivial, collective, bursty regime with avalanches. In the homogeneous case without disorder, the system synchronizes and the bursty behavior is reflected into a doubling-period transition to chaos for a two dimensional discrete map. Numerical simulations show that the bursty chaotic phase with avalanches exhibits a spontaneous emergence of time correlations and enhanced Kolmogorov complexity. Our analysis reveals a mechanism for the generation of irregular avalanches that emerges from the combination of disorder and deterministic underlying chaotic dynamics.

Networks of spiking neurons feature a wide range of dynamical collective behaviors, that are believed to be crucial for brain functioning [1]. Next to uncorrelated and asynchronous dynamics, quasi-synchronous phases and regimes of irregular activity have been observed, showing a still unexplained degree of correlation that could encode part of the neural function [2–7]. Understanding the mechanisms that generate such experimentally observed collective behaviors and the transition between them is a major goal in theoretical neuroscience [1, 8–15]. A particularly interesting dynamical signature of collective irregular regimes is that of *avalanches* or bursts of spiking neurons with heavy-tailed distributions of activity [6, 16, 17]. Interestingly, in cortical networks, irregular activity at the collective level [18, 19] and avalanches characterized by power-law distributions have been widely observed both *in vitro* and *in vivo* [20–23]. These regimes are thought to be closely related to information processing in the cortex [24–26] and to adaptive [27] and healthy [28] behavior.

Several mechanisms leading to irregular dynamics and bursts in networks of spiking neurons have been proposed. Irregular dynamical phases have been related to a balance between excitatory and inhibitory inputs [29, 30] or to a disorder in the network or in the couplings [11, 31] as crucial ingredients. Power-law distributed avalanches have been attributed to synaptic plasticity with a stochastic noise in the charging [32–36] or to dynamical mechanisms inspired by self-organized criticality (SOC) [27, 37, 38]. The balance between excitation and inhibition plays an important role in the latter dynamical regime as well [39], and a relation between uncorrelated dynamics in a network of stochastic units and power-law scaling has been proposed [40, 41].

In this Letter we show that correlated irregular dynamics can be observed in homogeneous deterministic networks of N identical purely excitatory spiking neurons endowed with synaptic plasticity, coupled by an all to all, mean field (MF), interaction. In this case, all neurons are synchronized but, for small enough synaptic decay time, the system displays a doubling-period transition from a periodic to a chaotic phase.

Such a transition can be analytically described by studying the competition among the system timescales in the strong and weak coupling limits, and, in the limit of vanishing synaptic decay time, by reducing the dynamics to a one-dimensional map. In the presence of disorder, e.g. considering a degree based mean field in the couplings, we show that the dynamics exhibits three phases, depending on the interaction strength and synaptic decay time. In particular, in addition to the quasi periodic-periodic and the asynchronous regimes [42], a phase characterized by power-law distributed avalanches emerges in correspondence to the chaotic phase of the homogeneous MF model. Chaos is preserved in this dynamical phase, as confirmed by the computation of the Lyapunov exponents, and it is characterized by the onset of strong temporal correlations and high complexity. Our analysis uncovers a connection between stability properties and emergent avalanche activity in the presence of short-term synaptic plasticity, that may go beyond our particular case of study.

We consider a disordered random network of leaky integrate-and-fire (LIF) neurons [43] connected via the Tsodyks-Uziel-Markram (TUM) model for short term synaptic plasticity [44]. We describe it by a Degree Based Mean Field approximation (DMF) [42, 45], that has been shown to reproduce the relevant features of the collective dynamics of this model. Neurons are labeled by the index $i = 1 \dots N$ and they are characterized by their coupling constant gk_i, randomly extracted from $P(k_i)$, the distribution of couplings in the network. Nk_i can be

interpreted as an effective in-degree which, in this framework, represents the only relevant topological feature of the structure and it justifies the DMF name. For each node i, we define three differential equations:

$$\dot{v}_i(t) = a - v_i(t) + gk_iY(t) \tag{1}$$

$$\dot{y}_i(t) = -\frac{y_i(t)}{\tau_{in}} + u(1-y_i(t)-z_i(t))S_i(t) \tag{2}$$

$$\dot{z}_i(t) = \frac{y_i(t)}{\tau_{in}} - \frac{z_i(t)}{\tau_R}, \tag{3}$$

where $v_i(t)$ is the membrane potential of neuron i while $x_i(t)$, $y_i(t)$ and $z_i(t)$ represent the available, active and inactive resources respectively, of the corresponding synapses (with the normalization $x_i + y_i + z_i = 1$). The potential is reset to 0 at times $t_i(m)$ when it reaches the threshold $v_i(t_i(m)) = 1$. At $t_i(m)$, a spike activates a fraction u of the available resources, and the activation is modeled as a spike train $S_i(t) = \sum_m \delta(t - t_i(m))$. Finally, in the DMF approach, the incoming synaptic current can be written as a sum of active resources $Y(t) = N^{-1}\sum_{i=1}^{N} y_i(t)$.

Equations (1, 2, 3) are characterized by three time scales: the period of the oscillating non interacting neuron $T = \log(a/(a-1))$, the recovery time τ_R and the synaptic decay time τ_{in}. Numerical simulations of the model can be performed very efficiently by introducing an event driven map [42, 46]. The regime $\tau_{in} \lesssim T$ has been studied in detail in [47], and it features a transition from a quasi-synchronous to an asynchronous phase as a function of g and of the shape of the coupling distribution $P(k_i)$.

Here we will focus instead on the regime $\tau_{in} \ll T \ll \tau_R$, setting $a = 1.3$, $\tau_R = 10$ and varying τ_{in} between 10^{-1} and 10^{-5}. These parameter values are consistent with those selected in [44], where they have been chosen on the basis of biological motivations.

Mean Field (MF). The presence of a further non trivial phase can be put into evidence by considering the simple in-degree distribution $P(k_i) = \delta(k_i - k_0)$. In this fully mean field (MF) case, where all the coupling constants are equal, all neurons become completely synchronized after an initial transient state, as can be verified numerically. Hence, Equations (1, 2, 3) reduce to the equations of a single neuron with coupling k_0, with $Y(t) = y(t)$. The dynamics can be rewritten as a simple event driven map in z_n and y_n, representing the inactive and active resources before the n-th firing event (see Supplemental Material):

$$y_{n+1} = e^{-\frac{\Delta_n}{\tau_{in}}}(y_n + u(1-y_n-z_n)) \tag{4}$$

$$z_{n+1} = -e^{-\frac{\Delta_n}{\tau_{in}}}\frac{y_n + u(1-y_n-z_n)}{1-\tau_{in}/\tau_R} + e^{-\frac{\Delta_n}{\tau_R}}\left(z_n + \frac{y_n + u(1-y_n-z_n)}{1-\tau_{in}/\tau_R}\right), \tag{5}$$

where the time interval Δ_n between the n-th and the $(n+1)$-th firing event is obtained from Equation:

$$1 = a - e^{-\frac{\Delta_n}{\tau_{in}}}\frac{g\tau_{in}k_0(y_n + u(1-y_n-z_n))}{1-\tau_{in}} - e^{-\Delta_n}\left(a - \frac{g\tau_{in}k_0(y_n + u(1-y_n-z_n))}{1-\tau_{in}}\right). \tag{6}$$

When $\tau_{in} \ll T \ll \tau_R$, an insight on the dynamics can be achieved by considering the opposite regimes of weak and strong interaction, i.e. when $gk_0Y(t)$ or $a - v_{k_0}(t)$ are negligible in equation (1), respectively. In both extreme regimes, the map in Eq.s (4-6) can be solved, and it features a periodic fixed point solution (see Supplemental Material for details). In particular, in the weak coupling regime, the periodicity is trivially T, and the interaction term remains negligible if $gk_0\tau_{in} \ll \tau_R/T$. On the other hand, if the $a - v_{k_0}(t)$ term can be ignored, the system (4-6) displays a much faster periodicity: $T_f = \tau_R/(gk_0\tau_{in})$ and the approximations holds only if $gk_0\tau_{in} \gg a\tau_R/\tau_{in}$.

In the region of the parameters $\tau_R/T \ll gk_0\tau_{in} \ll \tau_R/\tau_{in}$, neither the weak nor the strong coupling conditions are satisfied, and the competition between local and interacting terms, with slow or fast periodicity, plays a non trivial role destroying the presence of a periodic evolution. Such a behavior can be analyzed by means of the bifurcation diagram of Δ_n as a function of g at fixed τ_{in}. Figure 1 shows the presence of a stable fixed point for small and large values of g, describing the slow and a fast periodic regime, respectively. For an intermediate value, a period doubling first appears, then, at $g > g'(\tau_{in})$, the distribution of Δ_n becomes continuous. We observe indeed a transition to chaos as confirmed by the numerical calculation of the maximum Lyapunov exponent [48], which becomes positive at g' (see Supplemental Material). The Δ_n becomes again delta-distributed for $g > g''(\tau_{in})$. The phase diagram in Figure 4 shows that the τ_{in}-dependence of the boundaries of the chaotic phase, g', g'' (squares), is consistent with the continuous lines, obtained by the weak and strong coupling limit arguments. Taking the limit $\tau_{in} = 0$ with $g_{\text{eff}} = gk_0\tau_{in}$ constant in Eq.s (4-6), one obtains a single variable map as a function of g_{eff}, a and τ_R only, that can be studied analytically (see the Supplemental Material). This simpler map confirms the presence of a true chaotic dynamical phase.

Degree-based Mean Field (DMF). Let us now consider the multi-site DMF model with heterogeneous couplings extracted from a generic distribution $P(k_i)$ [49]. A relevant quantity describing the dynamical evolution and in particular the synchronicity level of the neurons is the Kuramoto parameter [50]: $R(t) = \frac{1}{N}\left|\sum_{i=1}^{N} e^{\imath\phi_i(t)}\right|$ where $\phi_i(t)$ is the phase of neuron i at time t:

$$\phi_i(t) = 2\pi\frac{t - t_i(m)}{t_i(m+1) - t_i(m)}, \tag{7}$$

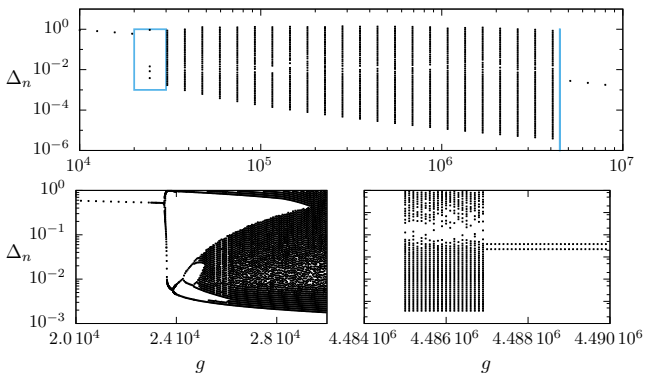

FIG. 1. Feigenbaum bifurcation diagram for the MF TUM model described by Eq.s (4-5) with $\tau_{in} = 10^{-3}$. The attractor for the interspike interval of the network Δ_n is showed as a function of the coupling constant g. Upper panel: bifurcation diagram in the full relevant range of the bifurcation parameter g. Lower-left panel: magnification on the period doubling cascade at the first transition. Lower-right panel: magnification on the second transition. The blue rectangles in the upper panel indicate the zooming regions corresponding to the lower panels.

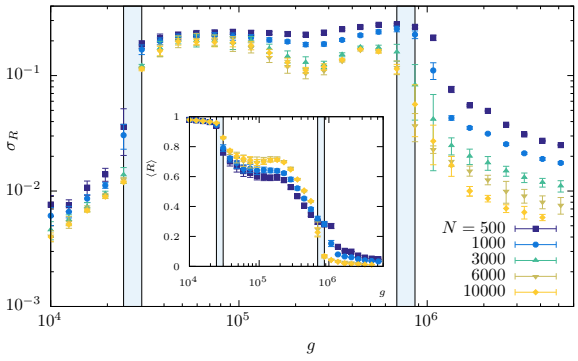

FIG. 2. (Color online) Standard deviation of the Kuramoto parameter, σ_R versus g for the DMF model with $\tau_{in} = 10^{-3}$ and five values of N. In the quasi-synchronous and bursty phases the data corresponding to the two larger values of N overlap within their statistical errors, indicating convergence in size, while deep in the asynchronous phase they decrease as $\sim N^{-1/2}$. Inset: temporal average of $R(t)$, showing that the larger sizes have attained their asymptotic value in all the phases. The vertical stripes are common to all the figures in the article and indicate the apparent discontinuity of $\langle R \rangle$ for the largest sizes.

where $t_i(m)$ is the m-th spike of neuron i and $t \in [t_i(m), t_i(m+1)]$. In Figure 2 the time average R of the Kuramoto parameter and its fluctuations are displayed as a function of g. At small couplings, $\langle R \rangle \approx 1$ and the fluctuations are small, as the systems is in a *quasi-synchronous* phase. At large g, $\langle R \rangle$ becomes very small ($\langle R \rangle \to 0$ with increasing N), consistently with a periodic *asynchronous* phase. In the irregular, *bursty*, regime, $\langle R \rangle$ exhibits moderate values and, more significantly, its fluctuations grow abruptly by an order of magnitude; this is a signal of a complex dynamical phase, illustrated in the raster plot in the inset of Figure 3. The fluctuations of $\langle R \rangle$ originate from the alternations of synchronous events with asynchronous phases characterized by smaller bursts where only a subset of the neurons fires simultaneously. The main plot of Figure 3 shows that the size s of such bursts, or avalanches, is broadly distributed (see the Supplemental Material for a detailed definition of burst size). Interestingly, the distribution is compatible with a power law $h(s) \sim s^{-\gamma}$ followed by a bump. The power γ, close to 2 (see the Supplemental Material), does not depend significantly on N, nor on g for a wide g-range in the bursty phase. Finally, the peaks at large s in the distributions correspond to synchronous events where all neurons fire quasi-simultaneously, and their position scale with the system size.

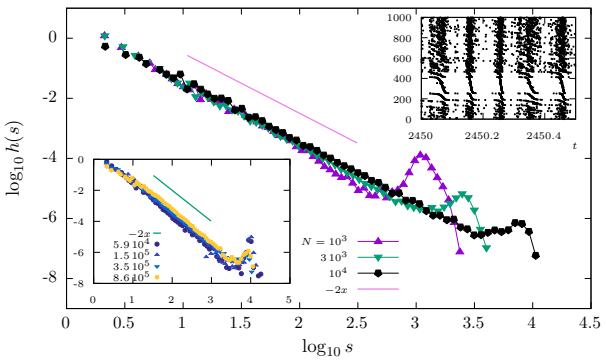

FIG. 3. (Color online) Avalanche size histogram $h(s)$ of the DMF model, $\tau_{in} = 10^{-3}$ and $g = 3.5{\cdot}10^5$ in the bursty regime, for several values of N. Upper inset: a fragment of the raster plot for the same system. Lower inset: $\log_{10} h(s)$ for $N = 10^4$ and various values of g across the bursty phase.

The natural issue is the relation between the chaotic phase in the single site MF model and the bursty-avalanche regime of the multi-site DMF approach. In the Supplemental Material we show that also the bursty phase is characterized by a chaotic dynamics with positive Lyapunov exponents. Moreover, in Figure 4 we have superimposed the dynamical phase diagrams of the MF and DMF models. In the DMF, the transitions points (circles) are set at the g intervals at which the abrupt increments of the fluctuations of the Kuramoto parameter take place (c.f. Fig. 2). In the MF case, the squares indicate the values of g at which the transitions to chaos occur. While the phase diagrams slightly differ, the phase diagram of the DMF model converges continuously to that of the MF model in the limit of vanishing width of the distribution $P(k_i)$, as illustrated numerically in the Supplemental Material. This result clarifies the deep connection between the chaotic nature of the dynamics of Equations (4-6) and the emergence of the bursty regime.

In the DMF model, the transition to the bursty

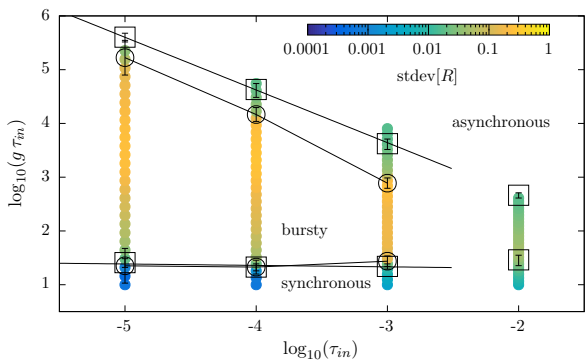

FIG. 4. (Color online) Dynamical phase diagram of the MF and DMF models in terms of the coupling constants g and of the synaptic time-scale $\tau_{\rm in}$. MF model: The squares indicate the g values at which the transition to chaos (along with the discontinuity of the interspike time standard deviation) takes place (see Supplemental Material). The black lines are linear fits. DMF model: Each colored point corresponds to a simulation, the color code indicating σ_R at the corresponding value of $(g, \tau_{\rm in})$. The intervals of g containing the discontinuity (c.f. Fig. 2) are signaled with black circles.

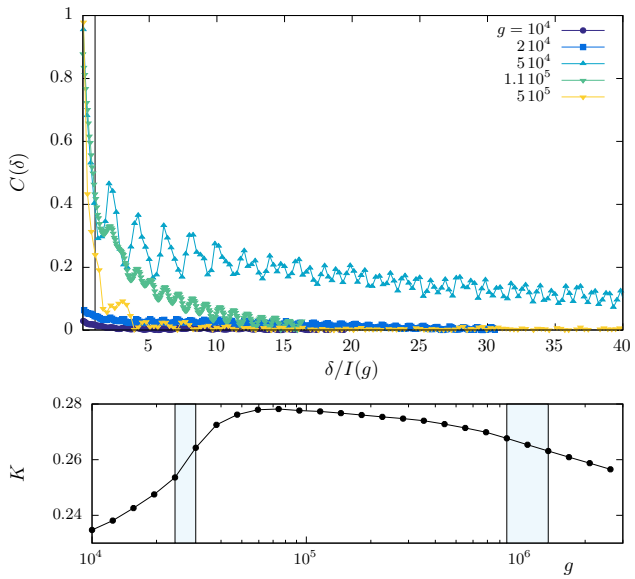

FIG. 5. (Color online) Upper panel: connected correlation function C as a function of the time difference δ in units of the average interspike time $I(g)$, for several values of g in the DMF model with $\tau_{in} = 10^{-3}$, $N = 800$. For values of g in the bursty phase, the correlation remains high even after large time differences. Lower panel: Kolmogorov Complexity of the DMF model, $\tau_{in} = 10^{-3}$, $N = 10^3$, and the spike time differences Δ_n stored with 14 digits of precision.

collective behavior also corresponds to the presence of large temporal correlations. We define the time-dependent *complex correlation*, $c(\delta, t) = (1/N)\sum_{i=1}^{N} e^{\imath\phi_i(t)} e^{-\imath\phi_i(t+\delta)}$, where $\phi_i(t)$ is the Kuramoto phase (7), along with the *connected correlation function*, $C(\delta) = |\langle c(\delta, t)\rangle_t| - |\langle c(\mathcal{T}, t)\rangle_t|$, as the temporal average $\langle\cdot\rangle_t$ of c over a sufficiently large interval of times t, minus its stationary value at a sufficiently large value of the time difference, $\delta = \mathcal{T}$ (for details at this regard see the Supplemental Material section). $C(\delta)$ measures in this way the average amount of correlation between spike configurations separated by a time-delay δ. The quantity $C(\delta)$ (see Fig. 5, upper panel) reveals the existence of large correlations for times δ much larger than the average interspike time, $I(g)$, only in the bursty regime (for $3 \cdot 10^4 \lesssim g \lesssim 10^5$ at $\tau_{in} = 10^{-3}$), while in the synchronous and asynchronous regimes, $C(\delta)$ decays faster to its asymptotic value.

Another interesting quantity in temporal series of neural firing patterns is the amount of information they can sustain. In information theory, the Kolmogorov Complexity (KC) of a data sequence determines the length of the minimum computer program generating it, hence being a measure of the sequence predictability [51]. KC has been related to the computational power of artificial neural networks [52], and used in the quantitative characterization of epileptic EEG recordings [53]. We consider the KC of the model raster plot, interpreting it as an estimation of the amount of information that can be codified in the dynamical signal (see the details of the KC estimation in the Supplemental Material section). The numerical results for the DMF model reveal that the KC as a function of g (see Fig. 5) is higher in the bursty regime, and it presents a maximum within the bursty regime (around $g \simeq 6\,10^4$ for $\tau_{in} = 10^{-3}$).

In summary, we have reported the existence of a new dynamical phase occurring in a network of purely excitatory LIF neurons connected with synaptic plasticity. This phase is strongly chaotic and it differs from previously known irregular phases for similar models, e.g. phases with chaotic transient dynamics [31, 54]. The chaotic phase must also be distinguished from previous irregular regimes observed in spiking neural models, namely *weak chaos* in purely excitatory disordered networks [55] or *stable chaos* in inhibitory ones [56–58]. The emergent dynamical regime occurs in a large region of the phase diagram, and it is separated by two dynamical transitions from the quasi-synchronous and asynchronous [47] regimes. Chaos is preserved in the presence of disordered couplings. In that case, interestingly, the chaotic phase also features characteristic power-law distributed avalanches. By properly defining temporal correlations and by using tools from information theory, we show that this additional phase is strongly correlated and it carries a relevant amount of information compared to the previously known, and less complex, dynamical phases.

We gratefully acknowledge the support of NVIDIA Corporation with the donation of the Tesla K40 GPU used for this research. We warmly thank S. di Santo, R. Livi, M. A. Muñoz and A. Politi for useful discussions.

* raffaella.burioni@fis.unipr.it

[1] T. P. Vogels, K. Rajan, and L. Abbott, Annu. Rev. Neurosci. **28**, 357 (2005).
[2] E. Hulata, V. Volman, and E. Ben-Jacob, Nat. Comput. **4**, 363 (2005).
[3] Y. Shu, A. Hasenstaub, and D. A. McCormick, Nature **423**, 288 (2003).
[4] X.-J. Wang, Physiol. Rev. **90**, 1195 (2010).
[5] A. Destexhe, S. W. Hughes, M. Rudolph, and V. Crunelli, Trends Neurosci. **30**, 334 (2007).
[6] J. Hesse and T. Gross, Front. Syst. Neurosci. **8** (2014).
[7] M. V. Sanchez-Vives and D. A. McCormick, Nat. Neurosci. **3**, 1027 (2000).
[8] L. F. Abbott and C. van Vreeswijk, Phys. Rev. E **48**, 1483 (1993).
[9] C. van Vreeswijk, Phys. Rev. E **54**, 5522 (1996).
[10] J. Kadmon and H. Sompolinsky, Phys. Rev. X **5**, 041030 (2015).
[11] N. Brunel, J. Comput. Neurosci. **8**, 183 (2000).
[12] C. Kirst, T. Geisel, and M. Timme, Phys. Rev. Lett. **102**, 068101 (2009).
[13] E. Montbrió, D. Pazó, and A. Roxin, Phys. Rev. X **5**, 021028 (2015).
[14] D. Hansel and G. Mato, Neural Comput. **15**, 1 (2003).
[15] S. Panzeri, R. S. Petersen, S. R. Schultz, M. Lebedev, and M. E. Diamond, Neuron **29**, 769 (2001).
[16] J. F. Mejias, H. J. Kappen, and J. J. Torres, PLoS ONE **5**, e13651 (2010).
[17] R. Livi, Chaos Soliton Fract. **55**, 60 (2013).
[18] B. D. Burns and A. C. Webb, Proc. R. Soc. B **194**, 211 (1976).
[19] M. London, A. Roth, L. Beeren, M. Hausser, and P. E. Latham, Nature **466**, 123 (2010).
[20] J. M. Beggs and D. Plenz, J. Neurosci. **23**, 11167 (2003).
[21] R. Segev, Y. Shapira, M. Benveniste, and E. Ben-Jacob, Phys. Rev. E **64**, 011920 (2001).
[22] T. Petermann, T. C. Thiagarajan, M. A. Lebedev, M. A. Nicolelis, D. R. Chialvo, and D. Plenz, Proc. Natl. Acad. Sci. U.S.A. **106**, 15921 (2009).
[23] S. El Boustani, O. Marre, S. Béhuret, P. Baudot, P. Yger, T. Bal, A. Destexhe, and Y. Frégnac, PLoS Comput. Biol. **5**, e1000519 (2009).
[24] O. Kinouchi and M. Copelli, Nat. Phys. **2**, 348 (2006).
[25] S. Ostojic, Nat. Neurosci. **17**, 594 (2014).
[26] M. Monteforte and F. Wolf, Phys. Rev. X **2**, 041007 (2012).
[27] D. R. Chialvo, Nat. Phys. **6**, 744 (2010).
[28] P. Massobrio, L. de Arcangelis, V. Pasquale, H. J. Jensen, and D. Plenz, Front. Syst. Neurosci. **9**, 22 (2015).
[29] D. J. Amit and N. Brunel, Cereb. Cortex **7**, 237 (1997).
[30] C. van Vreeswijk and H. Sompolinsky, Science **274**, 1724 (1996).
[31] J. M. Cortes, M. Desroches, S. Rodrigues, R. Veltz, M. A. Muñoz, and T. J. Sejnowski, Proc. Natl. Acad. Sci. U.S.A. **110**, 16610 (2013).
[32] A. Levina, J. M. Herrmann, and T. Geisel, Nat. Phys. **3**, 857 (2007).
[33] J. A. Bonachela and M. A. Muñoz, J. Stat. Mech. P09009 (2009).
[34] J. A. Bonachela, S. de Franciscis, J. J. Torres, and M. A. Muñoz, J. Stat. Mech. P02015 (2010).
[35] D. Millman, S. Mihalas, A. Kirkwood, and E. Niebur, Nat. Phys. **6**, 801 (2010).
[36] V. Volman, I. Baruchi, E. Persi, and E. Ben-Jacob, Physica A **335**, 249 (2004).
[37] L. de Arcangelis, C. Perrone-Capano, and H. J. Herrmann, Phys. Rev. Lett. **96**, 028107 (2006).
[38] S. di Santo, R. Burioni, A. Vezzani, and M. A. Muñoz, Phys. Rev. Lett. **116**, 240601 (2016).
[39] F. Lombardi, H. J. Herrmann, C. Perrone-Capano, D. Plenz, and L. de Arcangelis, Phys. Rev. Lett. **108**, 228703 (2012).
[40] J. Touboul and A. Destexhe, PLoS ONE **5**, e8982 (2010).
[41] J. Touboul and A. Destexhe, arXiv:1503.08033v4.
[42] R. Burioni, M. Casartelli, M. di Volo, R. Livi, and A. Vezzani, Sci. Rep. **4**, 4336 (2014).
[43] E. M. Izhikevich, IEEE Trans. Neural Networ. **15**, 1063 (2004).
[44] M. Tsodyks, A. Uziel, and H. Markram, J. Neurosci. **20**, 825 (2000).
[45] M. di Volo, R. Burioni, M. Casartelli, R. Livi, and A. Vezzani, Phys. Rev. E **90**, 022811 (2014).
[46] R. Brette, Neural Comput. **19**, 2604 (2007).
[47] M. di Volo, R. Livi, S. Luccioli, A. Politi, and A. Torcini, Phys. Rev. E **87**, 032801 (2013).
[48] G. Benettin, L. Galgani, A. Giorgilli, and J.-M. Strelcyn, Meccanica **15**, 21 (1980).
[49] Most of the numerical results presented in this article correspond to a Gaussian $P(k_i)$ with mean $\mu = 0.7$ and variance $\sigma = 0.077$.
[50] J. A. Acebrón, L. L. Bonilla, C. J. Pérez Vicente, F. Ritort, and R. Spigler, Rev. Mod. Phys. **77**, 137 (2005).
[51] M. Li and P. Vitányi, *An introduction to Kolmogorov complexity and its applications* (Springer, New York, 1993).
[52] J. L. Balcazar, R. Gavalda, and H. T. Siegelmann, IEEE Trans. Inf. Theory **43**, 1175 (1997).
[53] A. Petrosian, in *Proceedings of the Eighth IEEE Symposium on Computer-Based Medical Systems, Lubbock, Texas, 1995* (1995) p. 212.
[54] R. Zillmer, R. Livi, A. Politi, and A. Torcini, Phys. Rev. E **74**, 036203 (2006).
[55] S. Olmi, R. Livi, A. Politi, and A. Torcini, Phys. Rev. E **81**, 046119 (2010).
[56] R. Zillmer, N. Brunel, and D. Hansel, Phys. Rev. E **79**, 031909 (2009).
[57] E. Ullner and A. Politi, Phys. Rev. X **6**, 011015 (2016).
[58] D. Pazó and E. Montbrió, Phys. Rev. Lett. **116**, 238101 (2016).